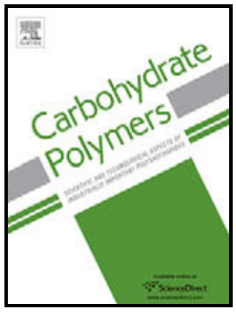


Title: Biodegradation of starch films: The roles of molecular and crystalline structure

Author: Ming Li Torsten Witt Fengwei Xie Frederick J. Warren Peter J. Halley Robert G. Gilbert

PII: S0144-8617(15)00013-2
DOI: http://dx.doi.org/doi:10.1016/j.carbpol.2015.01.011
Reference: CARP 9584

To appear in:

Received date: 23-9-2014
Revised date: 1-1-2015
Accepted date: 6-1-2015

Please cite this article as: Li, M., Witt, T., Xie, F., Warren, F. J., Halley, P. J., and Gilbert, R. G.,Biodegradation of starch films: The roles of molecular and crystalline structure, *Carbohydrate Polymers* (2015), http://dx.doi.org/10.1016/j.carbpol.2015.01.011

## Highlights

- The enzymatic degradation of starch films with varied structures is investigated.
- The molecular, crystalline and granular structures are varied using pre-treatments.
- Two degradation mechanisms are developed for the films with varied structures.
- Small starch molecules are more soluble and readily degradable by an enzyme.
- The retrograded structure inhibits enzymatic degradation.

# Biodegradation of starch films: The roles of molecular and crystalline structure

Ming Li,[a,b] Torsten Witt,[b] Fengwei Xie,[c] Frederick J Warren,[b] Peter J. Halley,[c,d] and Robert G. Gilbert[a,b,*]

[a] *School of Pharmacy, Huazhong University of Science and Technology, Wuhan, Hubei 430030, China*

[b] *The University of Queensland, Centre for Nutrition and Food Sciences, Queensland Alliance for Agriculture and Food Innovation, Brisbane, QLD 4072, Australia*

[c] *The University of Queensland, Australian Institute for Bioengineering and Nanotechnology, Brisbane, QLD 4072, Australia*

[d] *The University of Queensland, School of Chemical Engineering, Brisbane, QLD 4072, Australia*

*Corresponding author: R.G. Gilbert. Centre for Nutrition and Food Sciences, Queensland Alliance for Agricultural and Food Innovation, The University of Queensland, Brisbane, QLD 4072, Australia. Tel: +61 7 3365 4809, +86 186-7145-9682. E-mail: b.gilbert@uq.edu.au

Abbreviations: TPS, thermoplastic starch; ANOVA, analysis of variance; DMSO, dimethylsulfoxide; SEC, size-exclusion chromatography; NF, non-fractured; CF, cryo-fractured; LOS, log-of-slope

## Abstract

The influences of molecular, crystalline and granular structures on the biodegradability of compression-molded starch films were investigated. Fungal α-amylase was used as model degradation agent. The substrates comprised varied starch structures obtained by different degrees of acid hydrolysis, different granular sizes using size fractionation, and different degrees of crystallinity by aging for different times (up to 14 days). Two stages are identified for unretrograded films by fitting degradation data using first-order kinetics. Starch films containing larger molecules were degraded faster, but the rate coefficient was independent of the granule size. Retrograded films were degraded much slower than unretrograded ones, with a similar rate coefficient to that in the second stage of unretrograded films. Although initially the smaller molecules or the easily accessible starch chains on the amorphous film surface were degraded faster, the more ordered structure (resistant starch) formed from retrogradation, either before or during enzymatic degradation, strongly inhibits film biodegradation.



**Keywords**

starch; molecular structure; crystallinity; enzymatic degradation; bioplastic

# 1. Introduction

Starch-based biodegradable plastics are economic, abundant and renewable. In addition, starch's excellent biocompatibility leads to use in biomedical applications, such as tissue scaffolds (Gomes, Ribeiro, Malafaya, Reis & Cunha, 2001) or implants (Araujo, Cunha & Mota, 2004). These starch-based materials are frequently chemically or physically modified (Cristina Freire, Fertig, Podczeck, Veiga & Sousa, 2009; Herman & Remon, 1989; Singh & Nath, 2013) to obtain better mechanical (Chaudhary, Miler, Torley, Sopade & Halley, 2008), drug load and delivery properties (Cristina Freire, Fertig, Podczeck, Veiga & Sousa, 2009; Herman & Remon, 1989). Their degradation behavior is important to obtain controlled-release or to reduce the time required for the plastic to disappear from the environment; studies on the influence of specific starch structures on the films degradation can help to design starch materials for different purposes with desirable degradation rates.

The digestion kinetics of starch, and blends of starch/synthetic polymers (such as poly(vinyl alcohol), PLA or cellulose acetate) have been extensively reviewed and studied (Danjaji, Nawang, Ishiaku, Ismail & Mohd Ishak, 2002; Russo, Truss & Halley, 2009; Singh, Dartois & Kaur, 2010; Yew, Mohd Yusof, Mohd Ishak & Ishiaku, 2005). In this study we focus on the degradation kinetics of a series of starch films using a novel first-order kinetic approach (Butterworth, Warren, Grassby, Patel & Ellis, 2012) which has not previously been applied to the degradation of starch films, and which permits the identification of multiple kinetic processes during film degradation, allowing a greater mechanistic understanding of the behavior of these complex systems.

This model is applied to a series of starch films with tailored molecular, crystalline and granular structures purpose-designed to enable a truly systematic study the factors affecting the biodegradation rates of thermoplastic starch (TPS) materials. It is these structures which are expected to the dominant features controlling material functional properties (Li, Xie, Hasjim, Witt, Halley & Gilbert, 2015). We aim to determine whether it is lower- (chemical structure, molecular weight and molecular size distributions) or higher-order (crystallinity) structures that influence degradation kinetics of TPS films. Such a tailor-made series with systematic variation of three different structural levels has not been used previously for this purpose.

*In-vitro* enzymatic degradation by fungal α-amylase was used in this study to hydrolyze starch films with these different molecular, crystalline and granule structures in order to understand the effect of different structures on enzymatic degradation. Samples with a range of different levels of starch structure were compression-molded into thermoplastic starch films. Starches with different molecular sizes were obtained by acid hydrolysis of normal maize starch in alcohol solution; starch with different granular size distributions were obtained by water sedimentation. Native normal maize starch films were further retrograded to obtain different degrees of crystallinity. These samples were then enzymatically degraded.

Enzymatic degradation gives insights into degradation mechanisms (Gorrasi & Pantani, 2013) and may also be of use for ranking and screening biodegradability. Enzymatic degradation is more repeatable (Hamdi, Ponchel & Duchêne, 1998) and time-efficient (Russo, Truss & Halley, 2009) compared to field testing (Rudnik & Briassoulis, 2011; Sawada, 1994), as it is difficult to control the environmental factors

such as temperature, pH, humidity and microbe populations (Müller, 2005) in the latter methods. Bacteria and fungi are commonly involved in plastic biodegradation. Here a commercial fungal α-amylase is used, which is in the key group of enzymes (Azevedo, Gama & Reis, 2003) involved in starch film degradation.

# 2. Materials and Methods

## *2.1. Starch granules with different molecular sizes and their characterization*

### *2.1.1. Acid-alcohol treatment and destructuring of the crystalline structure*

Normal maize starch (amylose content of 28 %, as measured in a previous study (Vilaplana, Hasjim & Gilbert, 2012)), New Zealand Starch Ltd., Auckland, New Zealand) was acid-hydrolyzed following a procedure described by Tizzotti *et al.* (Tizzotti, Sweedman, Schäfer & Gilbert, 2013) with some modifications: 20 g of starch was suspended in 24.75 mL of alcohol to which 0.25 mL of HCl 37% solution was added. Starch was hydrolyzed under three conditions, a methanol/isopropanol mixture (v:v of 4:6) at 23 °C and 45 °C, and a pure isopropanol solution at 23 °C. The hydrolyzed starches were denoted $M_{23MI}$, $M_{45MI}$ and $M_{23I}$, respectively. The mixtures were stirred for 7 days, allowing the starch to reach a stable degree of hydrolysis (Robyt, Choe, Hahn & Fuchs, 1996). The reaction was stopped by adjusting the solution pH to 7.0 using 2.0 M NaOH and then washed with ethanol. Ethanol was removed by sedimentation for 5 min, then the hydrolyzed starch was dried in a vacuum oven at 45 °C for 24 h. 8 g of the hydrolyzed starch was dissolved in 100 mL dimethyl sulfoxide (DMSO; GR for analysis ACS, Merck & Co, Inc., Kilsyth, VIC, Australia) at 80 °C for an hour to remove any effect of crystalline structure on the enzymatic degradation. Dissolving in DMSO has been shown to completely disrupt the crystalline structure

(Mua, Rosowski & Jackson, 1997) without further unwanted molecular degradation (Han & Lim, 2004). The dissolved starch was then precipitated using ethanol (v:v of 1:6) followed by centrifugation for 5 min at 3000 *g*; this was repeated twice. The precipitated starch was dissolved in water at 60 °C, frozen using liquid nitrogen and lyophilized overnight using a BenchTop 2K freeze dryer (VirTis, Gardiner, NY, USA).

*2.1.2. Molecular size analysis*

The acid-hydrolyzed starches were dissolved in DMSO containing 0.5% wt LiBr (ReagentPlus, Sigma–Aldrich, Castle Hill, NSW, Australia) (DMSO/LiBr solution) with a concentration of 2 mg/mL, and analyzed in duplicate using size-exclusion chromatography (SEC) (Agilent 1100 series, Agilent Technologies, Waldbronn, Germany) with a refractive index detector (RID-10A, Shimadzu, Kyoto, Japan) following the method of Cave *et al*. (Cave, Seabrook, Gidley & Gilbert, 2009). The results were presented as the weight distributions of starch molecules as a function of hydrodynamic radius, denoted by $w(\log R_h)$ (Cave, Seabrook, Gidley & Gilbert, 2009). The average hydrodynamic radius ($\overline{R}_h$) of whole starch molecules (Level 2) was calculated as given elsewhere (Vilaplana & Gilbert, 2010).

***2.2. Starch granules with different granule sizes and their characterization***

*2.2.1. Starch sedimentation*

Sedimentation using the method of Dhital *et al.* (Dhital, Shrestha & Gidley, 2010) was chosen to obtain starch fractions with different granule size distributions while other structural features were not altered. A mixture of 10 g starch and 20 mL of deionized water was slowly poured into a 1 L measuring cylinder containing ~1 L

water. The contents were allowed to settle for 70, 30, and 15 min, and the fraction of the starch suspension remaining above a certain depth was removed by pipetting. The starch granules in each fraction were pelleted by centrifugation (3000 *g*, 5 min) and dried in the oven (40 °C), which were denoted as $G_{S70}$, $G_{S30}$ and $G_{S15}$. The sedimentation time $t$ was obtained from Stokes' law given by Eq. (1):

$$t = \frac{18\eta h}{g(\rho_s - \rho_w)d^2} \qquad [1]$$

where $\eta$ is the viscosity of water, $h$ is the sedimentation height, $g$ is the acceleration due to gravity, $\rho_s$ is the density of starch (1500 kg $m^{-3}$), $\rho_w$ is the density of water and $d$ is particle diameter.

*2.2.2. Granule size analysis*

The granular sizes of the three different fractions were measured using laser diffraction by a Mastersizer 2000 with Hydro MU (Malvern Instruments Ltd., Malvern, U.K.) following the method of Mahasukhonthachat *et al*. (Mahasukhonthachat, Sopade & Gidley, 2010). Approximately 250 mg of each of the different sedimented granule-size populations was dispersed in 5 mL of deionized water at least 30 min before the measurement to reduce granule aggregation. The obscuration measured by the instrument for all the measurements ranged from 10% to 15%. The particle size was measured in duplicate. The size of the different fractions is presented as surface-weighted mean [$D(3, 2)$] value, i.e. the diameter of a sphere that has the same volume: area ratio, assuming that the granules were homogenous spheres.

### *2.3. Compression molding, storage conditions and aged films with different degrees of crystallinity*

Starch with different structures ($M_{45MI}$, $M_{23I}$, $M_{23MI}$, $G_{S70}$, $G_{S30}$ , $G_{S15}$ and native starch) were compression-molded into starch films using a lab compression-molding machine at 135°C, with a pressure of 7.5 MPa for 5 min. Then the films were quench-cooled using a water cooling system to 35 °C before removal. A ratio of 2:3 glycerol / water was used as plasticizer, to obtain a plasticizer content of 30%. After releasing from the machine, starch films (35×60×0.5 $mm^3$) were immediately frozen with liquid nitrogen, and stored in a –80 °C Ultra-low Freezer (Sanyo Electric Co. Ltd) to minimize retrogradation, after which the film thickness was measured by microcaliper. All starch films had a thickness of ~0.5 mm.

After compression molding, starch films from native maize starch were sealed in plastic ziplock bags for 0, 8 and 14 days at room temperature to produce films denoted $C_{0D}$, $C_{8D}$ and $C_{14D}$. After the retrogradation step, the films were again stored in the –80 °C freezer to prevent further retrogradation.

### *2.4. Characterization methods*

#### *2.4.1. Scanning electron microscopy*

Starch films were manually fractured after being frozen in liquid nitrogen following the method used in a previous study (Li, Xie, Hasjim, Witt, Halley & Gilbert, 2015) to prevent any artifacts caused by cutting the film directly and to obtain clean internal surfaces. The fragments of films were coated with a thin layer of iridium using a MED-020 sputter coater (Leica Microsystems Pty. Ltd., Australia). The non-fractured (NF)

and cryo-fractured (Yokoyama, Renner-Nantz & Shoemaker) film surface morphologies were examined using a scanning electron microscope (SEM, JEOL XL30, Tokyo, Japan) at an accelerating voltage of 6 kV and a spot size of 6 nm.

*2.4.2. X-ray diffractometry*

The crystalline structure of starch films retrograded for different times was analyzed using a D8 Advance X-ray diffractometer (Bruker, Madison, WI, USA). The radiation parameters were set at 40 kV and 30 mA. The diffractograms were recorded over an angular range ($2\theta$) of 3–40°, with a step size of 0.02° and a step rate of 2 s per step. The degree of crystallinity was calculated from the diffractogram following the method of a previous paper (Li, Hasjim, Xie, Halley & Gilbert, 2014) using PeakFit software (Version 4.12 Systat Software, Inc., San Jose, CA, USA):

$$\text{Crystallinity (\%)} = \frac{\sum_{i=1}^{n} A_{ci}}{A_t} \times 100\% \qquad [2]$$

where $A_{ci}$ is the area under each crystalline peak with index $i$, and $A_t$ is the total area (both amorphous background and crystalline peaks) under the diffractogram. Each film was tested once; the standard deviation (Liu, Ramsden & Corke) of the XRD results is within 1–3 % as previously (Lopez-Rubio, Flanagan, Gilbert & Gidley, 2008).

*2.4.3. Enzymatic degradation and data fitting*

*In-v*itro degradation studies were performed on a piece of starch film (approximately 20 mg dry weight, with an area of 8 × 4 $mm^2$, thickness ~0.5 mm), cut from the film obtained in Section 2.3. These starch pieces were incubated in 3 mL of a sodium acetate

buffer (100 mM, pH 5, containing 5 mM calcium chloride) containing 83 U/mL fungal α-amylase from *Aspergillus niger* (Megazyme, Wicklow, Ireland) in a 50 mL centrifuge tube in a 23 °C shaking water bath (SWB20; Ratek Instruments Pty. Ltd., Boronia, VIC 3155, Australia) for 24 h. Supernatant (0.07 mL) was taken out of the degradation solution at defined time intervals from 0 to 1440 min. The incubation was halted by the addition of 0.63 mL of 0.2 M sulfuric acid. This mixture was centrifuged at 4000 *g* for 1 min, and 0.1 mL of supernatant from the centrifuged solution was further hydrolyzed by adding 0.1 mL of a solution of 28 U/mL amyloglucosidase (Megazyme, Wicklow, Ireland). The glucose concentration in the supernatant was determined using a D-glucose glucose oxidase-peroxidase (GOPOD) assay kit (Megazyme, Wicklow, Ireland) with a UV-VIS spectrophotometer (UV-1700 PharmaSpec, Shimadzu, Japan) to measure absorption at a wavelength of 510 nm.

Degradation (digestibility) curves were fitted with a first-order equation (Goñi, Garcia-Alonso & Saura-Calixto, 1997):

$$C_t = C_! \, (1 - e^{-kt}) \qquad [3]$$

Here $C_t$ is the starch degraded (expressed as mass per unit volume) at incubation time $t$, $C_!$ the corresponding amount of starch degraded at the end point of the reaction and $k$ the first-order degradation rate coefficient; this can be calculated using a form of the equation given by Butterworth *et al*. (Butterworth, Warren, Grassby, Patel & Ellis, 2012):

$$\ln \frac{dC}{dt} = \ln (C_! \, k) - kt \qquad [4]$$

223 $k$ was obtained by plotting ln(d$C$/d$t$) against $t$ and $C_\infty$ (Butterworth, Warren, Grassby,
224 Patel & Ellis, 2012). d$C$/d$t$ at the $i^{th}$ concentration $C_i$ was calculated as $(C_{i+2} - C_i)/ (t_{i+2}$-
225 $t_i)$, omitting the last two data points.

226 Deviations from linearity in this plot may result from various causes, the simplest of
227 which is the presence of more than one sequential rate process occurring during the
228 reaction, resulting in two (or more) linear regions. It has been demonstrated (Edwards,
229 Warren, Milligan, Butterworth & Ellis, 2014) that the degradation of structurally
230 complex starch substrates can be adequately described by the use of two sequential rate
231 processes, the rate coefficients for which are here termed here $k_1$ and $k_2$. Deviations
232 from a single straight line for plots fitted to Eq. (4) have been treated in this way here.

233 *2.4.4. Cold-water solubility*

234 Starch films were cut into 4 × 8 mm pieces (thickness of 0.5 mm) and immersed in 3
235 mL of 100 mM sodium acetate buffer adjusted to pH 5 using acetic acid, containing 5
236 mM calcium chloride. This was then incubated in a 23 °C shaking water bath for 22 h to
237 allow any soluble fractions to leach out. 0.1 mL of the supernatant was taken out from
238 the solution at various time intervals (0, 10, 30, 60, 90, 120 and 300 min) and was
239 degraded using 0.1 mL of 28 U/mL amyloglucosidase (Megazyme, Wicklow, Ireland).
240 The glucose content was analyzed with GOPOD reagent to find how much soluble
241 carbohydrate was dissolved.

242 ***2.5. Statistical analysis***

243 Statistical analysis was performed using Minitab 16 (Minitab Inc., State College, PA,
244 USA). ANOVA with Tukey's pairwise comparison was used to find the statistical

significance of differences between the cold-water solubility and degradation rates of the different starch films.

# 3. Results

## *3.1. Starch characteristics (before compression molding)*

### *3.1.1. Molecular structure of acid-hydrolyzed starch*

The degree of acid hydrolysis of starch is dependent on the type of solvent, reaction temperature and reaction time (Robyt, Choe, Hahn & Fuchs, 1996). Through this, the molecular size of starch can be controlled; the smallest molecules were produced in the methanol/isopropanol solvent at 45 °C, intermediate molecules from acid hydrolysis in pure isopropanol solvent at 23 °C, and the largest from methanol/isopropanol solvent at 23 °C. The resulting hydrolyzed starch molecules of $M_{45MI}$, $M_{23I}$, and $M_{23MI}$ had average hydrodynamic radii ($\overline{R}_h$) of 3.9, 5.4, and 12.9 nm, respectively, as calculated from the SEC size distributions, shown in Figure 1. Acid hydrolysis was stopped well before producing limit dextrins, and the molecules are expected to be largely random fragments (Hoover, 2000) from both amylopectin and amylose (Hasjim, Lavau, Gidley & Gilbert, 2010).

### *3.1.2. Granule size of sedimentation fractions*

Granule size distributions of the sedimentation fractions are shown in Figure 2 and the surface-weighted mean (diameter) [$D(3, 2)$] for both unfractionated normal maize starch granules and sedimentation fractions are in Table 1. The granular size distribution of each fraction ($G_{S70,}$ $G_{S30}$ and $G_{S15}$) was of course narrower than that of the

unfractionated native normal maize starch (Figure 2). The fractions with the longest sedimentation time ($G_{S70}$) showed the smallest surface-weighted mean, while $G_{S15}$ with the shortest sedimentation time showed the largest mean (which agrees with the calculated value based on Stokes' law with significantly different ($p$<0.05) surface-weighted mean values of granule sizes among the various sedimentation times.

### *3.2. Characteristics of films (after compression molding)*

#### *3.2.1. Morphology of starch films*

The unfractured and cryo-fractured morphologies of two films, $M_{45MI}$ and $C_{8D}$, were examined using SEM; typical images are shown in Figure 3. $M_{45MI}$ was used as an example of a completely amorphous starch film with no granular structure. Although $C_{8D}$ has undergone retrogradation, any remaining granular morphology will not be changed by this retrogradation, and thus $C_{8D}$ can serve as an example of the granular morphology of a typical starch film. After compression molding, the $M_{45MI}$ starch film made from amorphous acid-hydrolyzed starch displayed a smooth surface and homogenous internal structure, as shown by the images of the cryo-fractured and non-fractured surface, Figures 3A and B respectively. The cryo-fractured surface of $C_{8D}$ (Figure 3C) showed some structural remnants and cleavage planes due to fracture (see arrows). No granules could be observed on the surface or the interior of the $C_{8D}$ film: the untreated native starch granules were melted by the compression molding.

#### *3.2.2. XRD study of starch films*

The diffractograms of $C_{0D}$, $C_{8D}$ and $C_{14D}$ films are shown in Figure 4, from which the degrees of crystallinity of the starch films were found to be 4.7, 5.5 and 15.0 %

288 respectively. Immediately after compression molding ($C_{0D}$), two obvious sharp
289 diffraction peaks appeared at approximately 13 and 20°, representing V-type
290 crystallinity (Hasjim & Jane, 2009), due to the rapid recrystallization of amylose-lipid
291 and/or amylose-glycerol complexes. Comparing $C_{0D}$ and $C_{8D}$, there was only a small
292 increase in the total crystallinity after retrogradation. More B-type crystallinity formed
293 with strong reflections at $2\theta$ of about 17° (van Soest, Hulleman, de Wit & Vliegenthart,
294 1996) after retrogradation for 14 days, and the degree of crystallinity increased
295 significantly. The diffractograms of $M_{45MI}$, $M_{23I}$, and $M_{23MI}$ films were not examined, as
296 starch will be fully amorphous when it is dissolved in DMSO (Schmitz, Dona,
297 Castignolles, Gilbert & Gaborieau, 2009).

298 *3.2.3. Enzymatic degradation of starch films*

299 The log-of-slope (LOS) plots of the enzymatic degradation profile for the films with
300 no retrogradation ($M_{45MI}$, $M_{23I}$, $M_{23MI}$, $G_{S70}$, $G_{S30}$, $G_{S15}$ and $C_{0D}$) of the enzymatic
301 degradation profile exhibit two first-order stages (as shown in Figure 5A, which
302 represents the degradation of $M_{45MI}$ and as such is an example of the films with no
303 retrogradation), with two rate coefficients $k_1$ and $k_2$. Retrograded films ($C_{8D}$ and $C_{14D}$
304 films, Figure 5B) followed simple first-order kinetics with a single rate coefficient $k_1$.

305 The films without retrogradation ($M_{45MI}$, $M_{23I}$, $M_{23MI}$, $G_{S70}$, $G_{S30}$, $G_{S15}$ and $C_{0D}$ films)
306 were quickly degraded in the first 90 min (Figure 5B, C and D) the first rate coefficient
307 $k_1$ is given in Table 2. The second rate coefficient, $k_2$, was much smaller with relatively
308 large deviations due to the smaller enzymatic degradation rate. The values of $k_1$ were
309 significantly different among starch films with different molecular sizes: starch films
310 with larger molecules ($M_{23MI}$) were degraded more slowly. However, the values of $k_1$

were not significantly different among the films made from different granule sizes. This differs from what was reported in a previous study (Dhital, Shrestha & Gidley, 2010), that the rate coefficient had an inverse square relation with granule size for digestion of native starch granules. However, the difference between the morphology of the two systems is dramatic, the compression molding process used has disrupted the granular structure of the starch to a great enough extent that no difference could be detected between the different granular populations (this can be shown from the SEM results for the aged starch films (Figure 3)). As retrogradation will not change the granular morphology, the morphology of $C_{8D}$ film represents the morphology of a film with whole granular population, which shows no obvious granule boundaries or whole granules. An effect of granule size on the degradation rate might be observed if less effective compression-molding processes were used or if granular populations were more or less resistant to processing to a greater extent, as shown in wheat (Salman, Blazek, Lopez-Rubio, Gilbert, Hanley & Copeland, 2009). The second rate coefficient $k_2$ was essentially the same for all starches showing two degradation regimes; this value of $k_2$ was similar to the $k_1$ values of the retrograded $C_{8D}$ and $C_{14D}$ films. These results are consistent with conclusions from studies in the literature showing that crystallinity slows down enzyme degradation (Lopez-Rubio, Flanagan, Shrestha, Gidley & Gilbert, 2008; Shrestha, Ng, Lopez-Rubio, Blazek, Gilbert & Gidley, 2010).

The two regimes in appropriate LOS plots can be used to estimate different fractions ($C_\infty$) corresponding to the different degradation rates, $C_{\infty 1}$ and $C_{\infty 2}$, as shown in Table 2. Films with larger molecular sizes had a larger amount of substrate for the faster degradation stage; in addition, $C_{\infty 1}$ values for starch films with smaller molecules ($M_{45MI}$ and $M_{23I}$) were significantly smaller than for other films. The amounts of available

substrates for the fast degradation stage in other films took a large amount of the total weight and were not significantly different from each other. The value of $C_\infty$ is higher than the actual amount of degraded starch in Figure 5B, as it is the corresponding amount of starch degraded when the reaction was stopped, which may be not actually be 100% complete.

*3.2.4. Water solubility of starch films*

The amount of substrate leaching from a starch film into solution may affect the enzymatic degradation rate. Cold-water solubility of all the film was tested, and solubility profiles are shown in Figure 6. The cold-water solubility of retrograded starch films were the lowest, with only 0.2 % soluble starch at the end of the study (24 h) for the films retrograded for 8 and 14 days. For starch films produced with different granule sizes, the water solubilities of $G_{S70}$, $G_{S30}$ and $G_{S15}$ were 1.0, 0.44 and 0.50 %, respectively. There were no significant differences between the cold-water solubility of $G_{S30}$ and $G_{S15}$. Films produced from acid-hydrolyzed starches had the highest cold-water solubility, 2.3, 11.2, and 19.7 % soluble starch for $M_{23MI}$, $M_{23I}$, and $M_{45MI}$, respectively. Starch films made from acid-hydrolyzed starches displayed a rapid entry of starch molecules into solution in the first 90 minutes, whereafter the dissolution rate slowed down and reached a plateau after 120 min.

# 4. Discussion

The presence of two different kinetic regions during the degradation process indicates that there are at least two different degradation mechanisms, the first involving rapid degradation and the second involving slower degradation of more resistant

357 portions of the film. These two rates are best explored separately to try to understand
358 the underlying mechanics, before assessing what influence the interplay of the two has
359 on the film degradation.

360 The $k_1$ of the three films with different molecular sizes, $M_{45MI}$, $M_{23I}$, and $M_{23MI}$,
361 increased as the molecules become smaller. This increase in $k_1$ was matched by an
362 increase in the extent of dissolution for the smaller molecular components, as observed
363 previously (Hasjim, Li & Dhital, 2012). As the smaller molecules dissolved into
364 solution, there was an increase in available substrate for the enzyme and a subsequent
365 increase in the degradation rate. However, the cold-water solubility of small starch
366 molecules cannot be the only driver of increases in available substrate and subsequent
367 degradation rates. The starch films produced with $G_{S70}$, $G_{S30}$ and $G_{S15}$ sedimentation
368 fractions were degraded more rapidly than those from $M_{23I}$ and $M_{23MI}$, despite the films
369 prepared from acid hydrolyzed starches demonstrating significantly higher (2 – 10 %)
370 starch cold-water solubilities than the starch films from fractionated starches (0.5-1%
371 soluble starch). The high $k_1$ for $G_{S70,}$ $G_{S30}$ and $G_{S15}$ films must then be related to the
372 surface of the starch film having a greater susceptibility to enzyme attack, as they are
373 degraded rapidly despite leaching very little material into solution. The increase in the
374 amount of amorphous material at the surface of a film was strongly correlated with the
375 binding efficiency of the α-amylase, and therefore the degradation rate. The amorphous
376 surface structure of solid starch systems influences the rate of degradation (Butterworth,
377 Warren & Ellis, 2011). The reasons why the $k_1$ of the amorphous $M_{45MI}$, $M_{23I}$, and $M_{23MI}$
378 films was smaller than for $G_{S70,}$ $G_{S30}$ and $G_{S15}$ films will be explained later.

379 The slower degradation of the retrograded starch films was related strongly to the
380 length of retrogradation time. This explains the mechanism of the second degradation
381 step. $C_{0D}$ displayed both $k_1$ and $k_2$ while $C_{8D}$ and $C_{14D}$ films display only one rate, that
382 was indistinguishable from the $k_2$ of $C_{0D}$. The difference in retrogradation time brings
383 about a change within the film structure, reducing the fraction of rapidly degraded
384 starch through rearranging the amorphous structure into the B-type crystallites
385 displayed in $C_{8D}$ and $C_{14D}$ films. The increase in the crystalline structure has reduced the
386 availability of starch within the film for rapid digestion; thus the $C_{8D}$ and $C_{14D}$ films
387 were digested with a single, slow digestion rate coefficient, while all other films tested
388 had an initial faster rate coefficient.

389 The reduced degradation rate coefficient ($k_2$) in the films formed may be related to
390 retrogradation during enzymatic degradation. As reported by Lopez-Rubio *et al*.
391 (Lopez-Rubio, Flanagan, Shrestha, Gidley & Gilbert, 2008), a more ordered structure
392 formed during the enzymatic digestion of the high amylose starch extrudate and a
393 higher crystallinity was detected using XRD. Thus for the granular starches, the reduced
394 rate may be due to both the absence of rapidly digestible starch species, and the
395 retrogradation during the enzymatic process. Compared to the retrogradation during
396 enzymatic degradation, acid hydrolysis can lead to a higher degree of retrogradation
397 (Wang, Truong & Wang, 2003), as the increased mobility afforded to the starch chains
398 due to acid hydrolysis allows them to retrograde more rapidly. For $M_{23MI}$, which has
399 few cold-water soluble small molecules (2.3%), $k_1$ is reduced to a value similar to that
400 of the $C_{0D}$ film (without retrogradation). This in contrast to $M_{45MI}$ and $M_{23I}$ which show
401 an increased rate of degradation due to the presence of more small soluble molecules.
402 The influence of the small molecules can be crudely observed with $C_{\infty}1$ (Table 2), as $k_1$

for both $M_{45MI}$ and $M_{23I}$ accounting for a smaller portion of the total digestion than any other film, making the degradation kinetics of both of these films complex due to the effect of small soluble molecules as well as retrogradation. Finally, the trend for extent of digestion of the starches follows that of retrogradation rate and the length of time that the films were stored at room temperature. That is, $M_{45MI}$ and $M_{23I}$, being more rapidly retrograded, are digested to a lesser extent than $M_{23MI}$, just as $C_{8D}$ and $C_{24D}$ are digested less fully than $C_{0D}$.

The degradation of the films therefore occurs in two stages: (1) the degradation of easily accessible components, such as small molecules entering solution (as with $M_{45MI}$, $M_{23I}$, and $M_{23MI}$), or the degradation of easily accessible components that are integral to the film ($G_{S70}$, $G_{S30}$, $G_{S15}$and $C_{2D}$) represented by $k_1$; and (2) the degradation of the rest of the underlying resistant film structure, which occurred in all films with varying degrees, which is represented by $k_2$. The interplay of the two mechanisms is most obvious in the differences of the degradation rate coefficients of the films made with different molecular species: the solubilization and retrogradation occurred simultaneously in films with hydrolyzed molecules. The overlap of these two mechanisms during degradation may lead to the decrease in $k_1$. Thus the $k_1$ values of $M_{45MI}$, $M_{23I}$ and $M_{23MI}$ were significantly different among each other; $M_{23MI}$ displayed a smaller $k_1$ than $G_{S70}$, $G_{S30}$ and $G_{S15}$ films, where the faster degradation took a dominant role in the degradation of $G_{S70}$, $G_{S30}$, and $G_{S15}$ films.

## 5. Conclusions

Enzymatic degradation using fungal α-amylase on starch films with ranges of different molecular, crystalline and granular structures demonstrates strong effects of

426 starch structure on the kinetics. The initial rapid degradation of easily accessible starch
427 molecules was ascribed to two mechanisms: (1) the presence of small molecules that
428 enter solution and are rapidly degraded and (2) the likely presence of highly disordered
429 and accessible chains at the film surface that are more susceptible to degradation.
430 However, the presence of smaller molecules which may retrograde more rapidly and the
431 resistant structures formed during retrogradation, significantly reduce degradation rate.

## 432 Acknowledgements

433 We thank Mr. Wei Zou, Mr. Soon Ket Chong, Miss Oiwan Mo, and Mr. Leif
434 Sharkey for their kind help during the experiment, and thank Dr. Jovin Hasjim for proof
435 reading. The authors would like to thank the staff in the Centre for Microscopy and
436 Microanalysis at The University of Queensland, a node of the Australian Microscopy
437 and Microanalysis Research Facility (AMMRF). Financial assistance from an
438 Australian Research Council Discovery grant, DP130102461, is appreciated, as is the
439 support of the 1000-Talents Program of the Chinese Foreign Experts Bureau.

440

# References


Araujo, M. A., Cunha, A. M., & Mota, M. (2004). Changes in morphology of starch-based prothestic thermoplastic material during enzymatic degradation. *Journal of Biomaterials Science Polymer Edition, 15*(10), 1263-1280.

Azevedo, H. S., Gama, F. M., & Reis, R. L. (2003). *In vitro* assessment of the enzymatic degradation of several starch based biomaterials. *Biomacromolecules, 4*(6), 1703-1712.

Butterworth, P. J., Warren, F. J., & Ellis, P. R. (2011). Human α-amylase and starch digestion: An interesting marriage. *Starch - Stärke, 63*(7), 395-405.

Butterworth, P. J., Warren, F. J., Grassby, T., Patel, H., & Ellis, P. R. (2012). Analysis of starch amylolysis using plots for first-order kinetics. *Carbohydrate Polymers, 87*(3), 2189-2197.

Cave, R. A., Seabrook, S. A., Gidley, M. J., & Gilbert, R. G. (2009). Characterization of starch by size-exclusion chromatography: the limitations imposed by shear scission. *Biomacromolecules, 10*(8), 2245-2253.

Chaudhary, A. L., Miler, M., Torley, P. J., Sopade, P. A., & Halley, P. J. (2008). Amylose content and chemical modification effects on the extrusion of thermoplastic starch from maize. *Carbohydrate Polymers, 74*(4), 907-913.

Cristina Freire, A., Fertig, C. C., Podczeck, F., Veiga, F., & Sousa, J. (2009). Starch-based coatings for colon-specific drug delivery. Part I: The influence of heat treatment on the physico-chemical properties of high amylose maize starches. *European Journal of Pharmaceutics and Biopharmaceutics, 72*(3), 574-586.

Danjaji, I. D., Nawang, R., Ishiaku, U. S., Ismail, H., & Mohd Ishak, Z. A. M. (2002). Degradation studies and moisture uptake of sago-starch-filled linear low-density polyethylene composites. *Polymer Testing, 21*(1), 75-81.

Dhital, S., Shrestha, A. K., & Gidley, M. J. (2010). Relationship between granule size and in vitro digestibility of maize and potato starches. *Carbohydrate Polymers, 82*(2), 480-488.

Edwards, C. H., Warren, F. J., Milligan, P. J., Butterworth, P. J. and Ellis, P. R. 2014. A novel method for classifying starch digestion by modelling the amylolysis of plant foods using first-order enzyme kinetic principles. Food & Function *5*(11), 2751-2758.

Gomes, M. E., Ribeiro, A. S., Malafaya, P. B., Reis, R. L., & Cunha, A. M. (2001). A new approach based on injection moulding to produce biodegradable starch-based polymeric scaffolds: morphology, mechanical and degradation behaviour. *Biomaterials, 22*(9), 883-889.

475 Goñi, I., Garcia-Alonso, A., & Saura-Calixto, F. (1997). A starch hydrolysis procedure
476 to estimate glycemic index. *Nutrition Research, 17*(3), 427-437.

477 Gorrasi, G., & Pantani, R. (2013). Effect of PLA grades and morphologies on hydrolytic
478 degradation at composting temperature: Assessment of structural modification and
479 kinetic parameters. *Polymer Degradation and Stability, 98*(5), 1006-1014.

480 Hamdi, G., Ponchel, G., & Duchêne, D. (1998). An original method for studying *in*
481 *vitro* the enzymatic degradation of cross-linked starch microspheres. *Journal of*
482 *Controlled Release, 55*(2–3), 193-201.

483 Han, J.-A., & Lim, S.-T. (2004). Structural changes of corn starches by heating and
484 stirring in DMSO measured by SEC-MALLS-RI system. *Carbohydrate Polymers,*
485 *55*(3), 265-272.

486 Hasjim, J., & Jane, J.-L. (2009). Production of Resistant Starch by Extrusion Cooking
487 of Acid-Modified Normal-Maize Starch. *Journal of Food Science, 74*(7), C556-C562.

488 Hasjim, J., Lavau, G. C., Gidley, M. J., & Gilbert, R. G. (2010). *In vivo* and *in vitro*
489 starch digestion: are current in vitro techniques adequate? *Biomacromolecules, 11*(12),
490 3600-3608.

491 Hasjim, J., Li, E., & Dhital, S. (2012). Milling of rice grains: The roles of starch
492 structures in the solubility and swelling properties of rice flour. *Starch - Stärke, 64*(8),
493 631-645.

494 Herman, J., & Remon, J. P. (1989). Modified starches as hydrophilic matrices for
495 controlled oral delivery. II. In vitro drug release evaluation of thermally modified
496 starches. *International Journal of Pharmaceutics, 56*(1), 65-70.

497 Hoover, R. (2000). Acid-treated starches. *Food Reviews International, 16*(3), 369-392.

498 Li, M., Hasjim, J., Xie, F., Halley, P. J., & Gilbert, R. G. (2014). Shear degradation of
499 molecular, crystalline, and granular structures of starch during extrusion. *Starch -*
500 *Stärke, 66*(7-8), 595-605.

501 Li, M., Xie, F., Hasjim, J., Witt, T., Halley, P. J., & Gilbert, R. G. (2015). Establishing
502 whether the structural feature controlling the mechanical properties of starch films is
503 molecular or crystalline. *Carbohydrate Polymers, 117*(0), 262-270.

504 Liu, H., Ramsden, L., & Corke, H. (1997). Physical properties and enzymatic
505 digestibility of acetylated ae, wx, and normal maize starch. *Carbohydrate Polymers,*
506 *34*(4), 283-289.

507 Lopez-Rubio, A., Flanagan, B. M., Gilbert, E. P., & Gidley, M. J. (2008). A novel
508 approach for calculating starch crystallinity and its correlation with double helix
509 content: a combined XRD and NMR study. *Biopolymers, 89*(9), 761-768.

510 Lopez-Rubio, A., Flanagan, B. M., Shrestha, A. K., Gidley, M. J., & Gilbert, E. P.
511 (2008). Molecular Rearrangement Of Starch During In Vitro Digestion: Toward A

Better Understanding Of Enzyme Resistant Starch Formation In Processed Starches. *Biomacromolecules, 9*(7), 1951-1958.

Mahasukhonthachat, K., Sopade, P. A., & Gidley, M. J. (2010). Kinetics of starch digestion in sorghum as affected by particle size. *Journal of Food Engineering, 96*(1), 18-28.

Mua, J. P., Rosowski, J. R., & Jackson, D. S. (1997). Initial phase solubilization of normal corn starch by methyl sulfoxide (DMSO): Evidence from scanning electron microscopy and size exclusion chromatography. *Starch - Stärke, 49*(10), 401-407.

Müller, R.-J. (2005). Biodegradability of polymers: Regulations and methods for testing. *Biopolymers online*: Wiley-VCH Verlag GmbH & Co. KGaA.

Robyt, J. F., Choe, J.-y., Hahn, R. S., & Fuchs, E. B. (1996). Acid modification of starch granules in alcohols: effects of temperature, acid concentration, and starch concentration. *Carbohydrate Research, 281*(2), 203-218.

Rudnik, E., & Briassoulis, D. (2011). Degradation behaviour of poly(lactic acid) films and fibres in soil under Mediterranean field conditions and laboratory simulations testing. *Industrial Crops and Products, 33*(3), 648-658.

Russo, M. A. L., Truss, R., & Halley, P. J. (2009). The enzymatic hydrolysis of starch-based PVOH and polyol plasticised blends. *Carbohydrate Polymers, 77*(3), 442-448.

Salman, H., Blazek, J., Lopez-Rubio, A., Gilbert, E. P., Hanley, T., & Copeland, L. (2009). Structure-function relationships in A and B granules from wheat starches of similar amylose content. *Carbohydrate Polymers, 75*(3), 420-427.

Sawada, H. (1994). Field Testing of Biodegradable Plastics. In D. Yoshiharu & F. Kazuhiko (Eds.). *Studies in Polymer Science* (Vol. 12, pp. 298-312): Elsevier.

Schmitz, S., Dona, A. C., Castignolles, P., Gilbert, R. G., & Gaborieau, M. (2009). Quantification of the Extent of Starch Dissolution in Dimethylsulfoxide by 1H NMR spectroscopy. *Macromolecular Bioscience, 9*(5), 506-514.

Shrestha, A. K., Ng, C. S., Lopez-Rubio, A., Blazek, J., Gilbert, E. P., & Gidley, M. J. (2010). Enzyme resistance and structural organization in extruded high amylose maize starch. *Carbohydrate Polymers, 80*(3), 699-710.

Singh, A. V., & Nath, L. K. (2013). Evaluation of chemically modified hydrophobic sago starch as a carrier for controlled drug delivery. *Saudi Pharmaceutical Journal, 21*(2), 193-200.

Singh, J., Dartois, A., & Kaur, L. (2010). Starch digestibility in food matrix: a review. *Trends in Food Science & Technology, 21*(4), 168-180.

Tizzotti, M. J., Sweedman, M. C., Schäfer, C., & Gilbert, R. G. (2013). The influence of macromolecular architecture on the critical aggregation concentration of large amphiphilic starch derivatives. *Food Hydrocolloids, 31*(2), 365-374.

549 van Soest, J. J. G., Hulleman, S. H. D., de Wit, D., & Vliegenthart, J. F. G. (1996).
550 Crystallinity in starch bioplastics. *Industrial Crops and Products, 5*(1), 11-22.

551 Vilaplana, F., & Gilbert, R. G. (2010). Two-dimensional size/branch length
552 distributions of a branched polymer. *Macromolecules, 43*(17), 7321-7329.

553 Vilaplana, F., Hasjim, J., & Gilbert, R. G. (2012). Amylose content in starches: Toward
554 optimal definition and validating experimental methods. *Carbohydrate Polymers, 88*(1),
555 103-111.

556 Wang, Y.-J., Truong, V.-D., & Wang, L. (2003). Structures and rheological properties
557 of corn starch as affected by acid hydrolysis. *Carbohydrate Polymers, 52*(3), 327-333.

558 Yew, G. H., Mohd Yusof, A. M., Mohd Ishak, Z. A., & Ishiaku, U. S. (2005). Water
559 absorption and enzymatic degradation of poly(lactic acid)/rice starch composites.
560 *Polymer Degradation and Stability, 90*(3), 488-500.

561 Yokoyama, W., Renner-Nantz, J., & Shoemaker, C. (1998). Starch molecular mass and
562 size by size-exclusion chromatography in DMSO-LiBr coupled with multiple angle
563 laser light scattering. *Cereal Chemistry, 75*(4), 530-535.

564

565

565

566 ## Figure Captions

567 Figure 1. SEC weight distribution of acid-alcohol treated starches.

568 Figure 2. Granular size distributions of different fractions from normal maize starch.

569 Figure 3. Non-fractured (NF) and cryo-fractured (Yokoyama, Renner-Nantz &
570 Shoemaker) surface morphologies of $M_{45MI}$ and $C_{8D}$ films (A, $M_{45MI}$-CF; B, $M_{45MI}$-NF;
571 C, $C_{8D}$-CF; D, $C_{8D}$-NF). Arrows indicate remnants and cleavage planes.

572 Figure 4. X-ray diffractograms of compression-molded normal amylose maize starch
573 after being stored for 0, 8 and 14 days ($C_{0D}$, $C_{8D}$, and $C_{14D}$).

574 Figure 5. Digestogram of different starch films (A, sample log of slope (LOS) plot of
575 $M_{45MI}$ starch degradation; B, $C_{0D}$, $C_{8D}$, and $C_{14D}$ are films with different retrogradation
576 time as presented in Figure 4; C, $M_{45MI}$, $M_{23I}$, and $M_{23MI}$ are films with acid hydrolyzed
577 molecules as shown in Figure 1; D, $G_{S70,}$ $G_{S30}$ and $G_{S15}$ are films from fractions with
578 different granule sizes as in Table 1).

579 Figure 6. Cold-water solubility of starch films with different structures as a function
580 of immersion time.

581

581 Table 1. Granule size distribution of fractionated normal maize starch (NMS =
582 unfractionated)

| Description | Sedimentation time (min) | *D* (3, 2) (μm) |
|---|---|---|
| $G_{S70}$ | 70 | 6.3 ± 0.2 C [a] |
| $G_{S30}$ | 30 | 13.1 ± 0 B |
| $G_{S15}$ | 15 | 16.1 ± 0 A |
| NMS | - | 7.6 ± 0.4 C |

583 [a] Numbers in the same column with different letters are significantly different at $p <$
584 0.05.

585

585 Table 2. Degradation rate coefficeints ($min^{-1}$) and degraded starch in different stages of

586 different starch films[a]

| Films | $k_1$ | $k_2$ | $C_{\infty}1$ | $C_{\infty}2$ |
|---|---|---|---|---|
| $M_{45MI}$ | 0.0167 ± 0.0011 D | 0.0009 ± 0.0004 A | 26.3 ± 1.4 B | 40.9 ±3.9 A |
| $M_{23I}$ | 0.0129 ± 0.0013 C | 0.0024 ± 0.0006 A | 30.4 ± 1.4 B | 38.2 ± 0.4 A |
| $M_{23MI}$ | 0.0073 ± 0.0007 B | 0.0019 ± 0.0009 A | 71.1 ± 18.0 AB | 29.6 ± 12.8 A |
| $C_{0D}$ | 0.0082 ± 0.0006 B | 0.0029 ± 0.0007 A | 87.3 ± 0.3 A | 25.2 ± 4.9 A |
| $C_{8D}$ | 0.0006 ± 0.0000 A | NA | 84.1 ± 13.6 A | |
| $C_{14D}$ | 0.0007 ± 0.0000 A | NA | 76.0 ± 7.0 AB | |
| $G_{S70}$ | 0.0168 ± 0.0017 D | 0.0022 ± 0.0006 A | 62.8 ± 5.3 AB | 15.1 ± 5.3 A |
| $G_{S30}$ | 0.0153 ± 0.0007 CD | 0.0015 ± 0.0002 A | 72.6 ± 13.1 AB | 15.3 ± 4.4 A |
| $G_{S15}$ | 0.0134 ± 0.0010 CD | 0.0023 ± 0.0006 A | 62.6 ± 2.8 AB | 22.4 ± 6.6 A |

587 [a] Numbers in the same column with different letters are significantly different at $p <$
588 0.05.
589

589

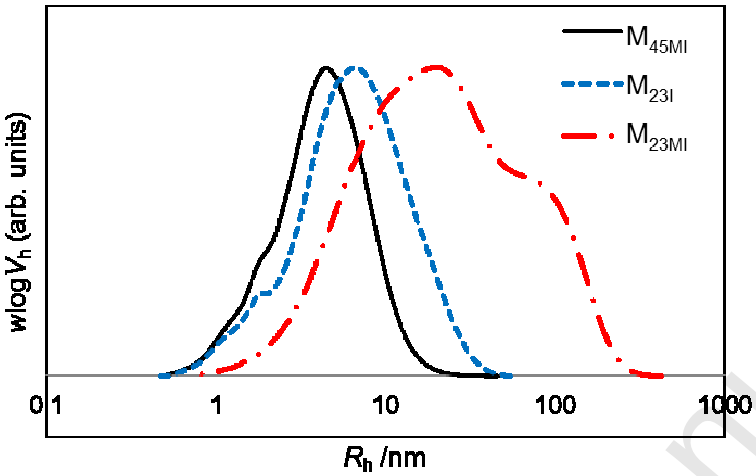


590

591 Figure 1.

592

592

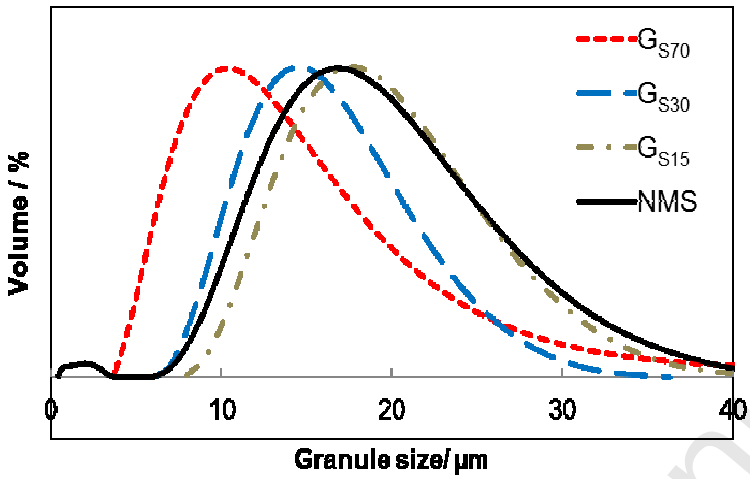


593

594 Figure 2.

595

595

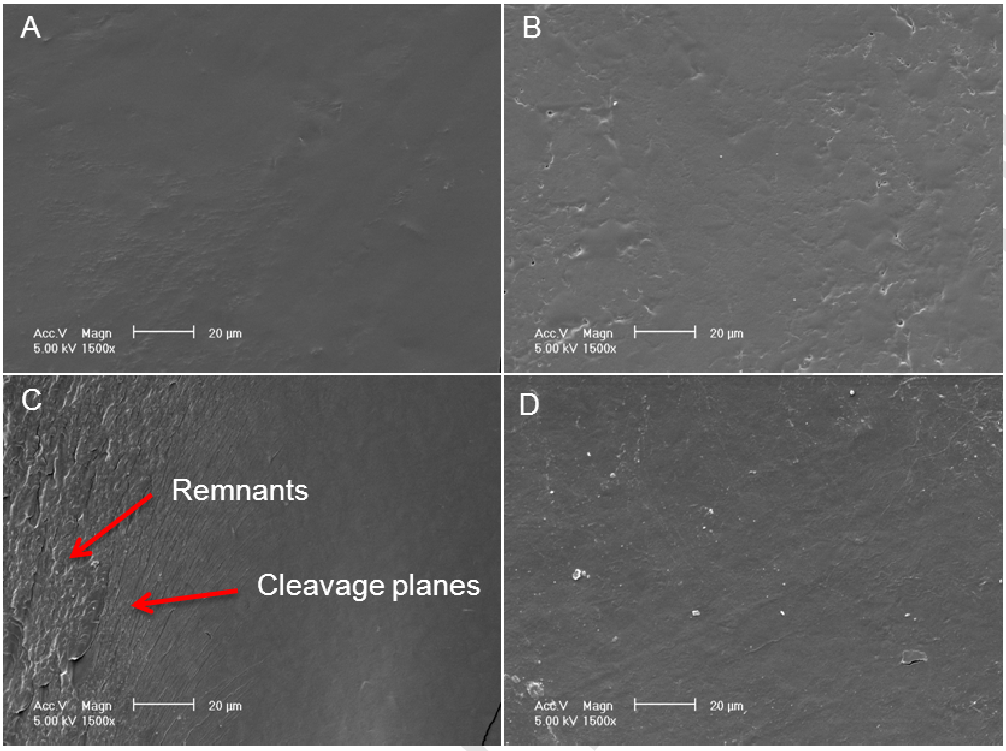


596

597 Figure 3.

598

598

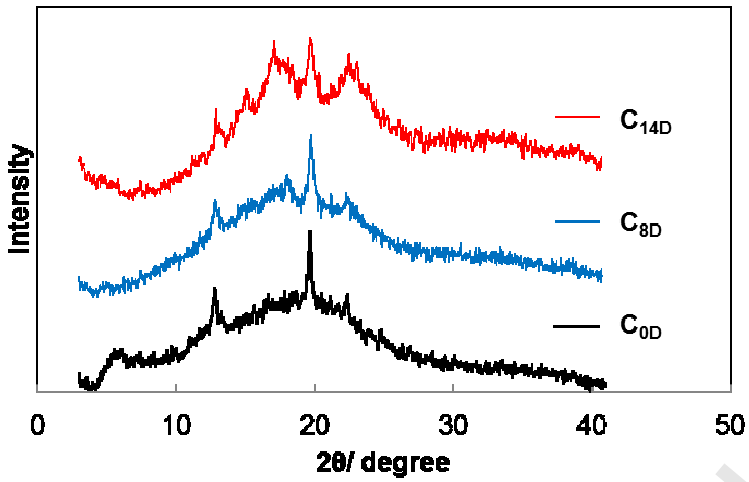


599

600 Figure 4.

601

601

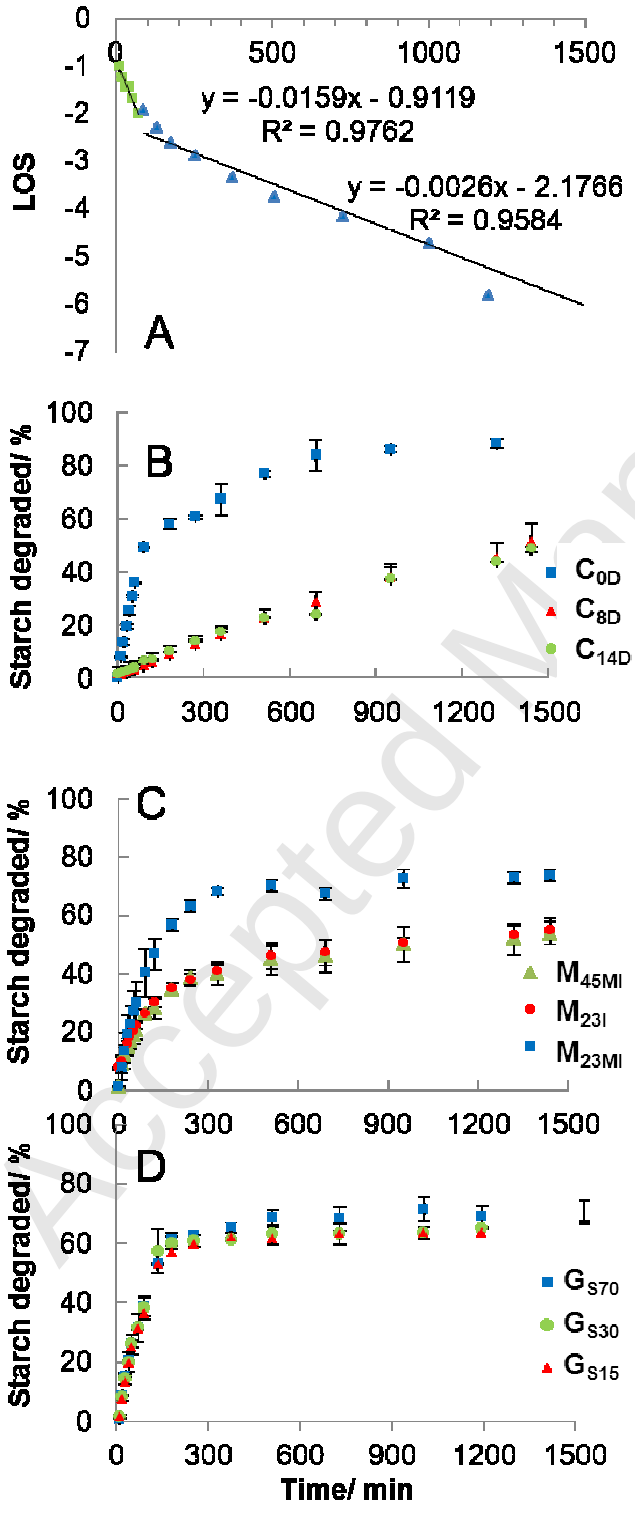


602

603 Figure 5.

604

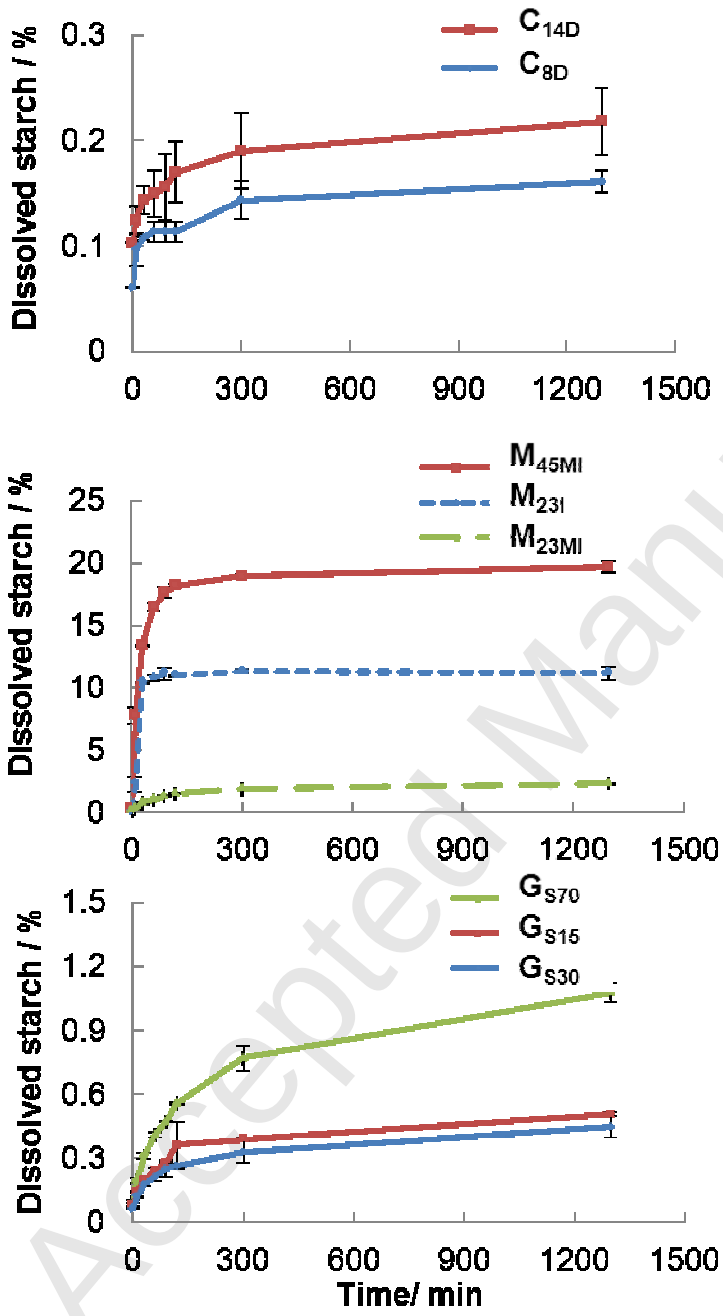


604

605 Figure 6.